Earth and Planetary Science Letters 323-324 (2012) 40–49

Contents lists available at SciVerse ScienceDirect

Earth and Planetary Science Letters

journal homepage: www.elsevier.com/locate/epsl

Chemical weathering response to tectonic forcing: A soils perspective from the San Gabriel Mountains, California

Jean L. Dixon *, Anthony S. Hartshorn [1], Arjun M. Heimsath, Roman A. DiBiase, Kelin X. Whipple

School of Earth and Space Exploration, Arizona State University, Tempe, AZ 85287, United States

ARTICLE INFO

Article history:
Received 30 July 2011
Received in revised form 3 January 2012
Accepted 9 January 2012
Available online 16 February 2012

Editor: R.W. Carlson

Keywords:
erosion
chemical weathering
soil production
kinetic limitation
tectonics

ABSTRACT

What controls the chemical weathering of soils in tectonically active landscapes? Recent field and modeling studies suggest that tectonic forcing and associated increases in erosion rates may either promote or hinder soil chemical weathering. These competing trajectories are dependent on two primary controls: the availability of fresh minerals and their residence time on the landsurface. Here, we explore rates and extents of soil weathering in the San Gabriel Mountains of California, where previous work has measured clear tectonic fingerprints on rates of long term exhumation, hillslope erosion and landscape morphology. We quantify chemical weathering across this landscape by elemental analysis of soils, saprolites and bedrock on six sites that bracket the low-gradient hillslopes of the relict upland plateau and the high-gradient hillslopes at the margins of the tectonically-driven incising landscape. Average chemical depletion fractions, which measure weathering losses from soil relative to unweathered parent material, decrease with increasing elevation and decreasing temperature, reflecting a combination of climate influence and potential dust inputs from the Mojave Desert. Weathering fluxes from non-dust-affected sites with similar elevations, climates and lithology correlate with both erosion rates and hillslope gradient. On low-gradient hillslopes (<25°), weathering rates increase with increasing erosion rates, reflecting the influence of mineral supply. However, on high-gradient hillslopes (>25°), weathering intensities and rates both decrease as erosion rates increase and soils thin. At the highest denudation rates (>300 t km^{-2} y^{-1}), saprolite production is outpaced, and soils are produced directly from fractured rock. These patterns are consistent with those predicted by a previously published model for denudation–weathering relationships based on mineral weathering kinetics. Variable weathering extents in soils indicate that weathering in the SGM is largely kinetically limited. This study is the first to quantify decreases in both rates and extents of soil chemical weathering with increasing erosion rates, and suggests tectonic uplift in rapidly eroding and incising landscapes may not stimulate increased silicate weathering.

1. Introduction

It is broadly understood that tectonic forcings influence the pace and pattern of landscape evolution by their control on landscape relief and the physical and chemical processes that move sediment and dissolve bedrock. Rock uplift drives river incision by lowering relative base level and therefore sets erosion rates at a landscape scale (Howard et al., 1994; Whipple and Tucker, 1999). Hillslopes, in turn, adjust to lower base levels by eroding more quickly and altering their morphology. This hillslope response can lag behind that of channels (Fernandes and Dietrich, 1997; Mudd and Furbish, 2007) resulting in transient landscapes with intermediate morphologies. Hillslope gradients and erosion rates are often correlated with modeled stream incision predicted by stream power laws (DiBiase et al., 2009; Ouimet et al., 2009). Furthermore, tectonic uplift controls rock strength through joint spacing and fractures that can strongly control erosion processes (Molnar et al., 2007). Despite much attention directed towards a landscape's physical responses to uplift, the chemical weathering response of hillslopes to tectonic forcing – and more importantly, to the associated changes in erosion rates, transport processes and morphology – remains poorly understood. The relationship between chemical weathering, erosion and uplift is essential to our understanding of long term climate variability and global carbon cycles. Silicate weathering may act as the major sink for atmospheric carbon dioxide over geologic time (e.g., Berner et al., 1983), and it has been suggested that tectonic uplift may drive CO_2 withdrawal by enhancing weathering (e.g., Ruddiman et al., 1997).

Rates of physical erosion and chemical weathering – specifically, mass loss by chemical dissolution – are positively correlated across diverse landscapes (Dixon et al., 2009b; Gaillardet et al., 1999; Hren et al., 2007; Millot et al., 2002; Riebe et al., 2004; Stallard and Edmond, 1983; West et al., 2005). Areas of fast uplift have some of

* Corresponding author at: Deutsches GeoForschungsZentrum GFZ, Section 3.4, Telegrafenberg, 14473 Potsdam, Germany. Tel.: +49 331 28611; fax: +49 331 2852.
E-mail address: jeannie@gfz-potsdam.de (J.L. Dixon).
[1] Present Address: Department of Geology and Environmental Science, James Madison University, Harrisonburg, VA 22807, United States.

0012-821X/$ – see front matter © 2012 Elsevier B.V. All rights reserved.
doi:10.1016/j.epsl.2012.01.010

the highest global riverine solute fluxes (Gaillardet et al., 1999; Waldbauer and Chamberlain, 2005) and soil weathering rates (Riebe et al., 2001), suggesting that tectonic uplift stimulates chemical weathering rates by increasing the supply of fresh minerals. Conversely, rapid uplift may also limit chemical weathering rates as erosion rates increase, soil residence times decrease, and weatherable minerals do not have sufficient time to weather completely (Riebe et al., 2004; Stallard and Edmond, 1983; West et al., 2005). In such a case, mineral weathering extent (the relative amount lost to dissolution) and rates (how rapidly mineral mass is lost) are limited by the kinetics of chemical reactions. Recent modeling studies (Ferrier and Kirchner, 2008; Gabet, 2007; Gabet and Mudd, 2009; Hilley and Porder, 2008; Hilley et al., 2010; Hren et al., 2007) indicate that soil weathering rates should be linearly coupled with denudation rates when limited by mineral supply, but shift to kinetic limitation as denudation rates increase and mineral residence times decrease. This relationship has been described as one of 'diminishing returns' (Gabet, 2007), such that the shift from *supply limitation* to *kinetic limitation* results in a decrease in the intensity of weathering and a decreasing slope to the relationship between predicted weathering rates and increasing rates of physical denudation (Fig. 1). At sufficiently high erosion rates, where the weathering zone is thin and mineral residence times are further decreased, the erosion–weathering relationship is predicted to become negative such that increases in erosion result in decreases in both weathering intensities and rates. In this last case, weathering reactions receive no further benefit from mineral supply, and are entirely controlled by weathering kinetics. We refer to this regime as *kinetic control* (Fig. 1).

While a number of studies have measured short term solute fluxes from streams draining major mountain belts (e.g., Gaillardet et al., 1999; Jacobson et al., 2003; Stallard and Edmond, 1983; West et al., 2005), relatively few studies have quantified the longer term chemical weathering signal from soils in rapidly eroding landscapes that are shaped by tectonics (Norton and von Blanckenburg, 2010; Riebe et al., 2001). Furthermore, field data have validated the supply limitation (Riebe et al., 2004) regime and suggested the kinetic limitation regime (Norton and von Blanckenburg, 2010), but the final kinetic control regime, where weathering rates decrease with increasing erosion rates, has not been explicitly quantified. Hillslopes in actively incising landscapes are promising settings to examine how rivers communicate increased uplift to hillslopes and how hillslopes, in turn, respond physically and chemically to changes in the tectonic signal. Here we quantify soil and bedrock chemical weathering in the San Gabriel Mountains of California, where landscape morphology and erosion rates reflect both the magnitude of and response time to tectonic forcing. In this landscape, we explore how slope, soil depth, erosion rates, and transport processes influence the downslope patterns of chemical weathering.

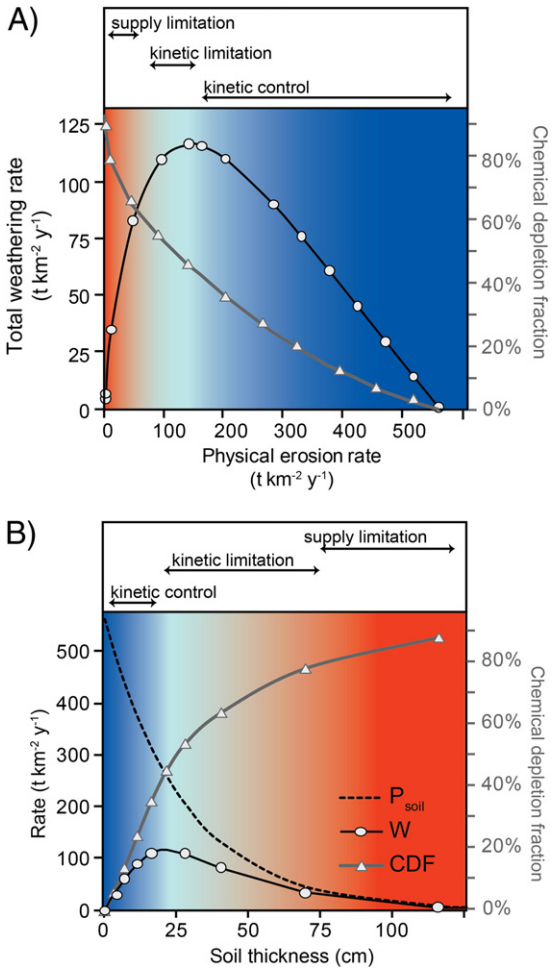

Fig. 1. Prediction for weathering vs. erosion using the model framework of Ferrier and Kirchner (2008). Weathering rates initially increase and later decrease as (A) erosion rates increase and (B) soil thicknesses decrease, marking the transition from *supply limitation* to *kinetic limitation* to *kinetic control*. Model inputs (Table A5) include dissolution rate constants, rock mineral abundances, and parameters that describe the degree to which soil production rates decrease with increasing soil thickness in the SGM (dotted line; Heimsath et al., in press). Weathering extents, shown as the chemical depletion fraction (CDF), decrease with increasing erosion rates and decreasing soil thickness, reflecting the decreasing influence of the supply of fresh minerals from soil production and increasing influence of shortened mineral residence times in a thinning weathering zone.

2. Field site and methods

2.1. Setting

The San Gabriel Mountains (SGM) in southern California (Fig. 2A) represent an ideal setting for quantifying hillslope responses to uplift across a transitional tectonic landscape. Compressional deformation associated with a large restraining bend in the San Andreas Fault has led to rates of exhumation determined by (U–Th)/He and apatite fission track thermochronology (Blythe et al., 2000, 2002; Spotila et al., 2002) and catchment-averaged denudation determined from ^{10}Be concentrations in river sands (DiBiase et al., 2009) that span orders of magnitude (10^1 to 10^3 m Ma^{-1}) and vary strongly with topography across the region. Denudation rates correlate with the magnitude of stream incision inferred from channel slope–area relationships and mean catchment gradient, and suggest a clear coupling between landscape morphology, erosion rates and the extent of tectonic forcing (DiBiase et al., 2009).

The SGM displays a morphology similar to other rapidly incised landscapes (e.g., Reinhardt et al., 2007), with low-relief, soil-mantled region that is separated from the bedrock-dominated, high-relief region by river knickpoints and an intermediate transient landscape. A slope map of the region highlights the position of these upland remnants of low relief amidst the incising landscape (Fig. 2B). Hillslopes in the low-relief, upland region are low-gradient and soil-mantled, and erode primarily by soil creep driven by bioturbation and tree-throw. At the margins of the low relief plateau and soil-mantled regions of the incised landscape, hillslopes display intermediate morphologies with broad low-gradient ridges that transition downhill to steep rocky soils as slopes exceed 20–30°. DiBiase et al. (2009) identified a critical slope of ~30°, above which erosion processes become detachment limited and slope failure may occur. On rapidly eroding portions of the landscape, hillslopes are bedrock-dominated with patchy soil cover and erode primarily by rock fall, debris flows and landslides (Heimsath et al., in press; Lavé and Burbank, 2004). Local denudation rates on soil-mantled portions of the SGM, derived from ^{10}Be concentrations in bedrock and saprolites beneath soil, are negatively correlated

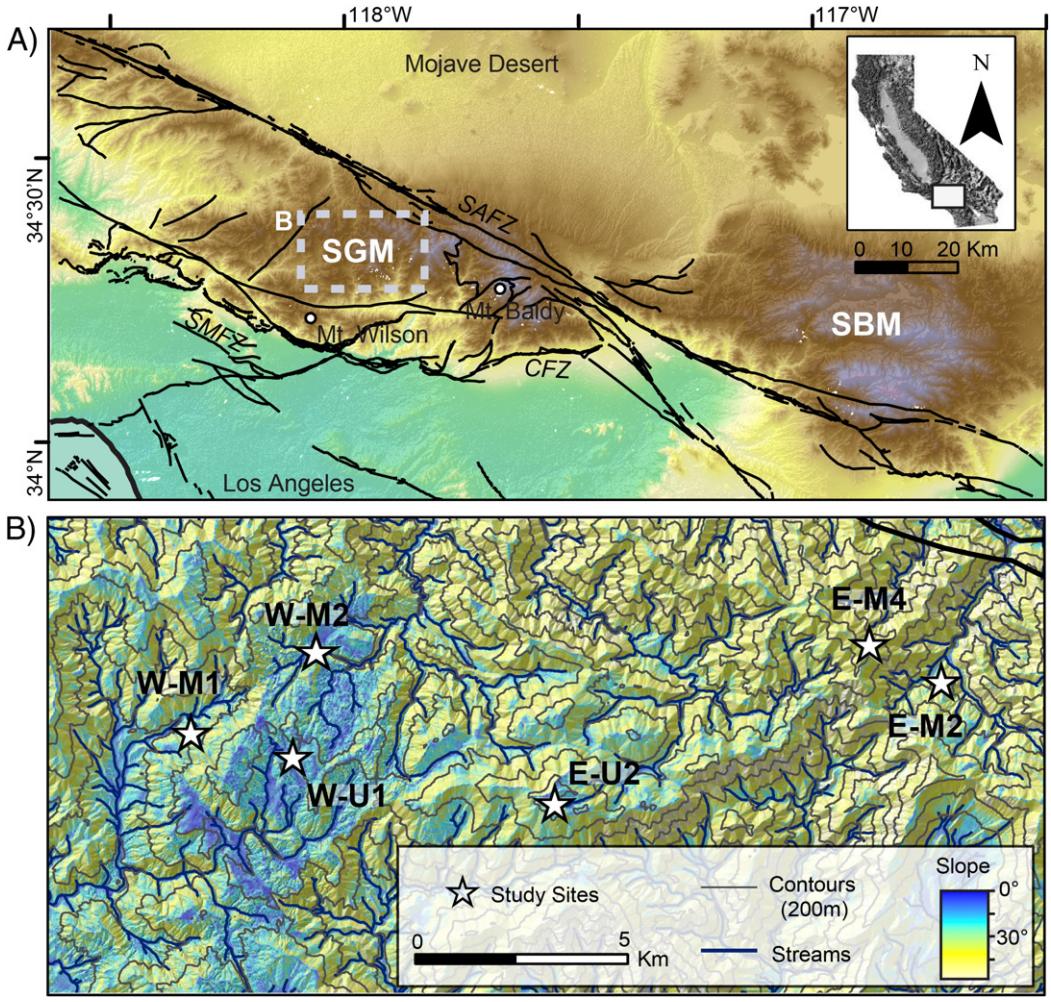

Fig. 2. (A) Overview elevation map (0–3500 m) of the San Gabriel Mountains (SGM), with inset map showing the location within California. The SGM are part of the California Transverse Range, which also including the San Bernadino Mountains (SBM). Black lines represent quaternary faults in major fault zones in the region: San Andreas Fault Zone (SAFZ), Cucamonga Fault Zone (CFZ), Sierra Madre Fault Zone (SMFZ). The dashed box shows the extent of map (B), a slope map of the western SGM showing locations of the six study sites.

with soil thickness (Heimsath et al., in press). The form of this relationship is different for soils found in the low relief (average slope > 30°) and high relief (average slope > 30°) portions of the landscape, suggesting that steeper landscapes have higher soil production rates than low-relief portions of the landscape with similar soil thicknesses. The soil production function describing the relationship for all soils in the SGM can be expressed as $P_{soil} = (567 \pm 21) * e^{(-0.036 \pm)}$ (Heimsath et al., in press), where P_{soil} is the soil production rate ($t\,km^{-2}\,y^{-1}$) and H is soil thickness (cm). This function identifies a maximum soil production rate of ~567 $t\,km^{-2}\,y^{-1}$ (218 m Ma^{-1}) under infinitely thin soils.

We selected six study sites across the SGM (Fig. 2B), choosing hillslopes that display morphologies and erosion processes associated with both the low-relief *upland* landscape and the *marginal* landscape transitioning to the more recent tectonic forcing. For ease of discussion, we refer to these hillslope categories as upland and marginal hillslopes. The two upland hillslopes (W-U1 and E-U2; Fig. 2B) are located within relict regions that do not appear to have adjusted to increased uplift and associated river incision. These sites are upstream of river knickpoints and composed entirely of low-gradient slopes (<20°). Along marginal hillslopes (W-M1, W-M2 and E-M3) located near or downstream of river knickpoints, slope increases with distance from the crest, and silty soils on low-gradient upslopes change rapidly as slopes exceed 20–30° to show a clear morphologic transition to rockier, planar slopes. These hillslope-scale observations complement the landscape scale observation of DiBiase et al. (2009) and Heimsath et al. (in press), who identified a similar process transition near 30°. Figure A1 in the supplementary material details hillslope morphologies and sample locations.

All sites overly granite (Morton and Miller, 2006; Yerkes and Campbell, 2005) and are unglaciated. Soils overlay fractured rock or a grussy saprolite (saprock) of indeterminate depth, although road cuts across the region suggest that saprolite mantles, where found, may be relatively thin (<2 m), grading to unweathered fractured bedrock. Vegetation in the region grades from chaparral at lower elevations to pine forests at higher elevations; chaparral is dominated by chamise (*Adenostoma fasciculatum*) and manzanita (*Arctostaphylos* spp.), while forests are dominated by Jeffrey Pine (*Pinus jeffreyi*). The Mediterranean climate is semiarid; mean annual precipitation (MAP; PRISM Climate Group 2009) ranges from 77 to 116 cm across the range, with mean annual temperatures (MAT) between 9 and 13 °C (Table 1). Because of the potential for orographic precipitation to influence hillslope denudation across the SGM, we selected sites at both low and high elevations across a west to east orographic gradient. We examined one upland site (E-U2) and one marginal site (E-M4) at the tops of Mt. Waterman and Mt. Williamson (2440 and 2500 m), respectively. In order to constrain the controls on weathering rates across morphologically different slopes as fully as possible, we focus much of our work on three western sites (W-U1, M1, M2) with similar lithology (Alf, 1948; Barth, 1990), elevation, climate and vegetation distinct from three eastern sites (E-U2, M3, M4) closer to the Mojave desert to the northeast.

Table 1
Location, climate, and morphology of study sites in the San Gabriel Mountains.

Site	Latitude (°N)	Longitude (°W)	Crest elevation (m)	MAT [a] (°C)	MAP [a] (cm)	Min. slope [b] (°)	Max. slope [b] (°)	Avg. slope [b] (°)
W-U1	34.347	118.003	1813	12.1	83	7	21	9
E-U2	34.336	117.936	2440	9.2	116	10	20	22
W-M1	34.352	118.029	1596	13.3	79	5	42	22
W-M2	34.369	117.998	1694	12.2	77	12	40	6
E-M3	34.364	117.837	1917	12.4	79	15	39	21
E-M4	34.372	117.858	2503	9.5	88	3	37	22

[a] Mean annual temperature (MAT) and precipitation (MAP) obtained from prism.oregonstate.edu (queried April 13, 2009) for each crest location.
[b] Minimum, maximum and average slope calculated from sampled locations in Table A4 of Supplementary material.

2.2. Field and laboratory methods

Our sampling and analysis follow the conceptual model for soils articulated by Dixon et al. (2009a) and built upon earlier work (e.g., Heimsath et al., 1999; Riebe et al., 2004). Soil is defined as the mobile mantle of physically transported material. It is produced by the disruption of bedrock or saprolite by biophysical processes such as bioturbation, frost heave, tree throw and root disturbance. Here, we do not distinguish between different weathering grades of saprolite or saprock, instead using the umbrella term saprolite for all weathered bedrock that is chemically altered and friable, but not physically disrupted, and therefore retains relict rock structure.

We sampled 4 to 6 soil profiles along transects extending downslope from the hillcrest or ridge at five sites in the San Gabriel Mountains. For a sixth site at Mount Williamson (E-M4), we sampled 8 soil profiles along hillslopes leading to tributaries of three major drainages (Big Rock Creek, Little Rock Creek and Bear Creek). Within each soil profile, we sampled bulk surface soils (<10 cm depth) and saprolite or bedrock at the base of each pit. We did not sample large rock fragments greater than gravel size (~5 cm) in soils, which are difficult to represent accurately within our sample size (~2–3 kg per sample), but which compose up to ~10% of soil mass on the steepest slopes. Soils were dried and subsampled for analysis. In total, we analyzed 55 soil samples from 34 locations, as well as 32 parent material (saprolite or rock) samples, for major oxides and Zr by X-ray fluorescence spectrometry (ALS Chemex, Reno, NV). Loss-on-ignition (LOI) was determined following combustion of a 5-g aliquot at 1000 °C for 1 h.

2.3. Calculations of chemical losses

We index elemental mass gains and losses to granite parent material (Brimhall et al., 1992; Chadwick et al., 1990) using immobile element concentrations. Parent material chemistry is determined based on average elemental chemistry of crystalline rock samples (discussed further in Section 4.2). Elements such as Zr and Ti are chemically immobile and enriched during weathering as other elements are removed from the rock and soil by dissolution. If they behave similarly, then the Ti–Zr ratio should remain fixed while both elements become enriched during weathering and mineral dissolution.

Changes in elemental concentrations that occur with weathering are reported as tau (τ_i) values, or mass transfer coefficients (Muir and Logan, 1982). These values represent the fractional mass gain ($\tau>0$) or loss ($\tau<0$) relative to parent material and are calculated as:

$$\tau_i = \left(\frac{i_{soil} * Zr_{rock}}{i_{rock} * Zr_{soil}} - 1\right), \tag{3}$$

where i_{soil} and i_{rock} are concentrations of element i in the soil and unweathered parent material, respectively, and Zr_{soil} and Zr_{rock} are the corresponding zirconium concentrations. All τ are calculated from bulk samples, including gravels larger than 2 mm. Elemental mass balances were adjusted by the fractional oxide composition and LOI.

We calculate the total fractional mass lost to chemical weathering as the Chemical Depletion Fraction (CDF) (Riebe et al., 2001):

$$CDF = \left(1 - \frac{Zr_{rock}}{Zr_{soil}}\right). \tag{4}$$

In actively eroding terrains the CDF represents the proportion of denudation that is accomplished by chemical weathering. One can also describe the fractional mass loss by conversion of rock to saprolite ($CDF_{saprolite}$) and saprolite to soil (CDF_{soil}) as:

$$CDF_{saprolite} = \left(1 - \frac{Zr_{rock}}{Zr_{sapolite}}\right) \tag{5}$$

and

$$CDF_{soil} = \left(1 - \frac{Zr_{saprolite}}{Zr_{soil}}\right). \tag{6}$$

Soil production rates (P_{soil}) were determined using the 'soil production function' determined for this region by Heimsath et al. (in press), using local ^{10}Be-derived rates of denudation:

$$P_{soil} = P_0 e^{-\alpha H} \tag{7}$$

Whereby P_0 is the maximum soil production rate in the region (567 ± 21 t km^{-2} y^{-1};), α is a fit constant (0.036 ± 0.002 cm^{-1}), and H is soil thickness (cm). This function describes the inverse relationship between soil thickness and ^{10}Be-derived local denudation rates (D), assuming soil production is balanced by denudation. These rates reflect the mass loss by both physical erosion (E) and chemical weathering (W), such that:

$$D = E + W. \tag{8}$$

The total chemical weathering rate (W) is calculated as the product of the CDF and the soil production rate (e.g., Riebe et al., 2004). The erosion rate is the difference between soil production and weathering (Eq. (8)). Total weathering can be separated into the component fluxes within soils (W_{soil}) and saprolites ($W_{saprolite}$), following the framework by Riebe et al. (2004). Here, we do not use the adapted equations from Dixon et al. (2009a) that are most appropriate in deeply weathered locations where mass loss occurs beneath the cosmogenic length scale (~120 cm in soils) because they assume cosmogenic-derived denudation rates do not capture weathering losses within the saprolite. Considering the thin soil depths and thin saprolite mantles (~1 m) in sampled sites of the SGM, the unaltered original equations from Riebe et al. (2004) are likely more appropriate in this setting; however, we note that this choice may result in the underestimation of weathering and erosion fluxes (Dixon et al., 2009a). Furthermore, soil weathering fluxes may be overestimated on the steepest and rockiest soils of sampled marginal hillslopes due to our exclusion of rare but present rock fragments of >5 cm in these soil samples.

2.4. Model of kinetic and supply limited weathering

We explore the predicted relationship between erosion and chemical weathering for San Gabriel soils using the numerical model of Ferrier and Kirchner (2008). This model predicts weathering fluxes from reaction kinetics and the combined role of erosion rates and soil depth in controlling the timescales of mineral dissolution. The model relies on the assumption that soil production rates decrease exponentially with soil thickness (e.g., Heimsath et al., 1997; Eq. (7)) and are balanced by erosion and weathering rates (Eq. (8)), and that the dissolution rate constant of a mineral is linearly dependent on its concentration in soil (Chamberlain et al., 2005). The steady-state concentration for a mineral in soil ($[X]_s$; mol g^{-1}) is a function of the initial concentration in bedrock ($[X]_r$), the dissolution rate constant (k_X; mol m^{-2} y^{-1}), mineral surface area (A_x; m^2 mol^{-1}) and the production rate (s_X; mol m^{-3} y^{-1}), such that:

$$[X]_s = \left(\frac{P_0\theta^{-\propto H}}{P_s H} * [X]_r + \frac{{}^{s}X}{\rho_s}\right) / \left(\frac{P_0\theta^{-\propto H}}{P_s H} + k_X A_X - \sum_{j=1}^{n}\left(k_j A_j \left[X_j\right]_s w_j - \frac{s_j w_j}{\rho_s}\right)\right). \quad (9)$$

In the summation term, 'j–n' describe the suite of minerals within soil and w_j is the molar mass (g mol^{-1}).

Chemical weathering rates (W) are then given as the sum of individual mineral weathering rates minus secondary mineral production:

$$W = H * \rho_s * \sum_{j=1}^{n}\left(k_j A_j \left[X_j\right]_s w_j - \frac{s_j w_j}{\rho_s}\right). \quad (10)$$

The important inputs to this model are the erosion rate, concentrations of major minerals in bedrock, the soil production function for the soils of interest, and dissolution rate constants. The steady-state weathering rate, soil mineral concentrations, and soil thickness are then solved iteratively. See Ferrier and Kirchner (2008) for more specific details on the model parameters and equations.

3. Results

3.1. Parent material chemistry

Zirconium and titanium concentrations in soils at three sites in the western SGM (Fig. 3A) are higher than corresponding concentrations within sampled bedrock. Two of the western sites, where soils directly overlie saprolites, lacked sampleable unweathered bedrock (W-U1 and W-M1). Soils from these sites show Ti–Zr ratios that are roughly similar to bedrock chemistry from W-M2 (Fig. 3A), suggesting that this bedrock reflects unweathered parent material for the nearby sites. We use the average element concentrations in these rock samples as bedrock composition at W-U1, W-M1 and W-M2 (Eqs. (3), (4) and (5)) and use parent material directly underlying soils to represent saprolite chemistry (Eqs. (5) and (6)). Relationships between Ti and Zr concentrations for individual sites in the eastern SGM are less clear (Fig. 3B), and we see no consistent trend that reflects a weathering signal. Heterogeneous parent material resulting from variable bedrock mineralogy or dust deposition may complicate the signature of weathering on immobile element concentrations (Ferrier et al., in press), and we discuss this possibility later in Section 4.2. Raw elemental data for soils, saprolites, and bedrock are provided in Tables A1–A3 within the Supplementary material.

3.2. Soil weathering

Measured CDFs range from −0.07 to 0.61 and average 0.32 ± 0.03 (± 1 SE) across the region (Table A4 of supplementary material). The majority of chemical losses from soils occur by Si loss, and τ_{Si} and τ_K are highly correlated with CDF ($r^2 = 0.98$ and 0.91, respectively). On

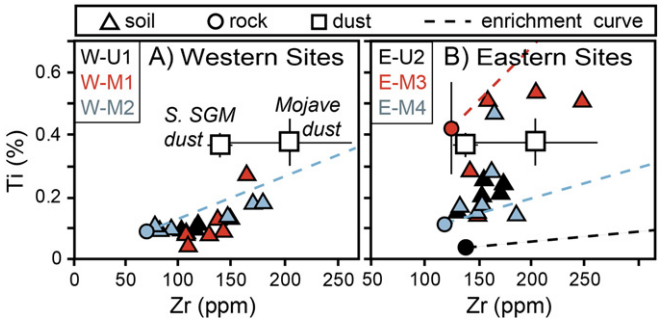

Fig. 3. Immobile element concentrations in rock (circles) and soil (triangles) sampled across study sites in the western SGM (A) and eastern SGM (B). As weathering removes dissolved mass from bedrock and soils, zirconium and titanium concentrations should be enriched similarly (dotted lines reflect enrichment curves extending from average bedrock compositions). Soils and bedrock concentrations at western sites roughly follow enrichment curves derived from bedrock composition at site SG-M2, while individual eastern sites show greater variability and less clear correlations between immobile element concentrations and weathering. The chemistry of dust sampled by Reheis and Kihl (1995) at sites in the southwestern SGM (near Mt. Wilson; dust sites 51–53) and the Mojave desert to the northeast (dust sites 25–31) are shown by open squares (error bars reflect standard deviation).

average, low-gradient sample locations of both upland and marginal hillslopes have CDFs that are 60% higher (0.34 ± 0.04, n = 22) than CDFs on higher gradient (>25°) locations (0.23 ± 0.05), however this difference is only statistically significant if eastern and western sites are considered separately. CDFs and losses of Si typically increase with increasing distance from the crest along the low-gradient portions of hillslope transects. Along upslope portions of the W-U1, E-U2, W-M2, and E-M3 catenas, for example, τ_{Si} becomes more negative downslope as Si losses increase by 32, 92, 14, and 286% respectively. Only one site, W-M2, shows significantly higher CDF for low-gradient sampling locations (0.57, $p<0.01$) than high-gradient locations (0.16). Despite the fact that high-gradient and low-gradient slopes display similar average weathering extents, mass losses recorded by CDFs and τ_{Si} along all marginal hillslope transects (W-M1,W-M2 and E-M3) decrease immediately across slope transitions (by 25, 83 and 50% respectively) as gradients exceeded 20–30° (Figure A1 of supplementary material, Fig. 5).

Average soil chemical depletions negatively correlate with altitude (Fig. 4A). The highest elevation sites (E-U2 and E-M4) have the lowest average annual temperatures (Fig. 4B) and highest annual precipitation (Fig. 4C), and show significantly lower CDF (0.18 ± 0.04, $p = 0.04$) than lower-elevation sites (0.38 ± 0.04). Elevation differences in soil weathering are complemented by east to west differences across the range. We contrast the fractional mass changes in three elements between the eastern sites that all have elevations > 1900 m with the corresponding elemental changes for the lower elevation transects (<1900 m) in the western SGM (Fig. 5). Eastern high elevation sites also display less negative average tau-Si and tau-Na values than those of low elevation hillslopes, with 8 soil profiles showing net mass gains of K or Mg. The largest mass losses of K (60 and 80%) are for two E-M4 samples located on the southernmost portion of that mountain, where the soils could have been shielded from dust-laden winds. On average, soil K from low elevation locations average a loss of 55%.

4. Discussion

4.1. Downslope patterns of chemical weathering extents

Hillslope patterns of CDF, τ_{Si}, and τ_{Na} (Figure A1 of supplementary material) generally indicate that soil chemical weathering extents increase downslope on low-gradient hillslopes in the SGM. These patterns on upland hillslopes and upslope portions of marginal hillslopes are consistent with two mechanisms that may explain increased weathering

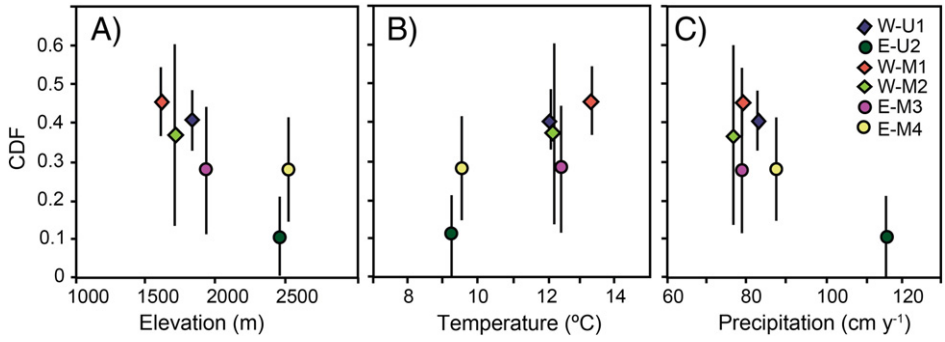

Fig. 4. Average chemical weathering losses from chemical depletion fractions (CDF) decrease with elevation (A), suggesting climate control by either temperature (B) or precipitation (C). Complicating matters, sites with lowest chemical depletions and therefore lowest soil weathering extents are higher elevation eastern sites (denoted by circles, while western sites are shown as diamonds) where slight differences in the granitoid lithology and deposition of Mojave-derived dust may play an important role in influencing weathering. Site descriptions provided in Table 1.

downslope. First, soils at greater distances from hillcrests have greater upslope contributing areas, implying increased water delivery from upslope for chemical weathering reactions. Second, while primary minerals weather upon vertical mobilization from parent rock into the soil column, they also weather during lateral transport downslope (Green et al., 2006; Yoo et al., 2007). Therefore, if soil weathering is kinetically limited, soils at distal but low-gradient parts of hillslopes could show greater extents of chemical weathering than crest soils due to longer hillslope residence times.

The progressive downslope increase in chemical weathering extents (as shown by CDF and tau values) along upslope portions of marginal hillslopes is disrupted as gradients increase rapidly from 20 to 30°, and soil weathering extents along all five hillslope transects decrease immediately downslope of these slope transitions. This sudden decrease in weathered extent is also visible for low elevation western sites when elemental taus are plotted against slope gradient (Fig. 5; see Section 4.2 for further discussion of elevational differences in weathering), and suggests that increased erosion rates and shorter soil residence times along marginal slopes may result in a decrease in chemical weathering.

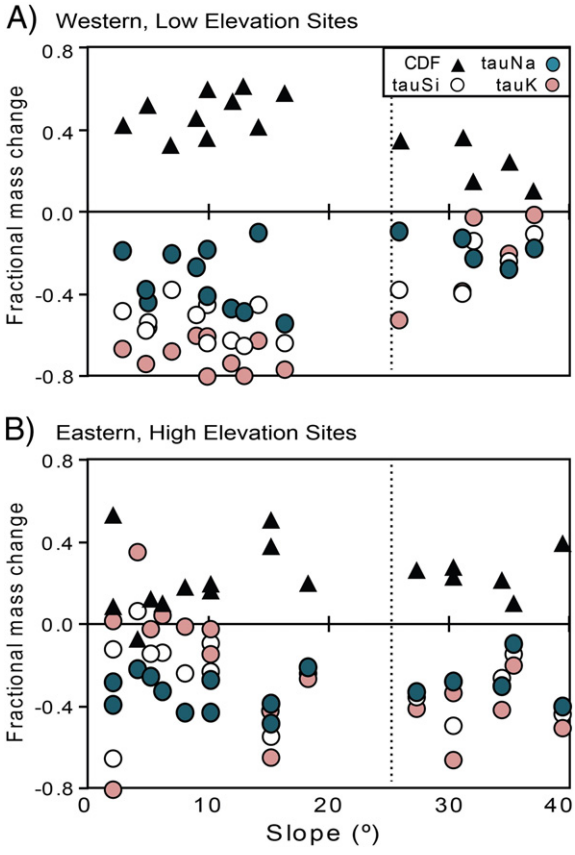

Fig. 5. Variability in losses of major cations at A) western low elevation sites (<1900 m) and B) eastern high elevation sites (>1900 m). Negative tau values represent losses and positive values represent net mass gains of individual elements. The dotted line represents the transition from low-gradient to high-gradient portions of marginal hillslopes at ~25°.

4.2. Climate, acidity and dust

Tectonic uplift has a broad morphologic and erosion rate imprint across the SGM, and appears to influence the patterns of soil chemical weathering extents at a hillslope scale; however, our data also show distinct extents and patterns of hillslope weathering at different elevations across the range. Prior empirical and mechanistic modeling of chemical weathering losses has used climate variables such as average air temperature and precipitation to explain patterns (e.g., White and Blum, 1995). Elevation is often invoked as a proxy for climate, and we find soil weathering losses (as shown by CDFs and elemental taus) decrease with increasing elevation and precipitation (Fig. 4A, C) and increase with increasing temperature (Fig. 4B). This relationship is strongly influenced by the two highest elevation sites (E-U2, M4) atop Mount Williamson and Waterman. A number of other elevation-dependent factors may also influence the rates and extents of soil weathering in the SGM. Anthropogenic acidity and dust deposition also likely vary with elevation in the SGM. Here, we explore the potential role these variables play in influencing the elevational patterns of weathering.

The San Gabriel Mountains have been called the most polluted montane region in North America. Aeolian inputs to these soils include anthropogenic acidity from the greater Los Angeles metropolitan area, which has been estimated to produce 33 g Nitrogen $m^{-2}\,y^{-1}$ (Riggan et al., 1985) and has the potential to influence soil weathering. Deposition rates measured near our six hillslopes (Kiefer and Fenn, 1997) as well as the California Air Quality model estimates (metadata, Tonnesen et al. 2007; 2002 raster data, R. Johnson, pers. comm.) both suggest average N inputs are <1 g N $m^{-2}\,y^{-1}$. Even if acid inputs to these soils were better constrained, few studies have examined the effects on chemical weathering of wet and dry HNO_3 deposition to rock and soil surfaces. In one study, NO_3^- levels meant to index nitric acid declined exponentially within 5 mm of the surface, but deposition rates were also greater if the substrate was wet (Padgett and Bytnerowicz, 2001), implying chemical weathering rates might increase with soil moisture. While it is possible that anthropogenic acidity may be catalyzing chemical weathering across the SGM, two lines of reasoning make it unlikely that the weathering extents and rates we report have been dominated by this nitrogen deposition. First, assuming that anthropogenic acidity levels first reached elevated levels 30 years ago, this

would only constitute a very small fraction (1–3%) of the residence times we estimate for hillslopes. Second, we find no evidence that decades of anthropogenic acid inputs to hillslopes have overprinted the sharp chemical weathering differences occurring between low- and high-gradient portions of hillslopes that we attribute to century- to millennial-scale processes. Despite the likelihood that acidity is not overprinting local trends in weathering, it is not clear whether it may result in broader differences between sites across the range.

Deposition of dust (either locally-derived or sourced from the Mojave Desert to the north) may also complicate soil chemistry in the SGM. Dust inputs have been found to reach up to 82% of weathering losses in some cases (Porder et al., 2007) and to offset weathering losses by their influence on soil chemistry (Ferrier et al., in press; Kurtz et al., 2001). Dust traps previously collected from three sites in the southern SGM east of Mt. Wilson (Reheis and Kihl, 1995) yielded estimated dust deposition rates of 13.3–39 g m^{-2} y^{-1}, including 9–20% from deposition of atmospheric salts. These dust fluxes represent 4–11% of the average soil production rate measured in the SGM (~360 t km^{-2} y^{-1}; Heimsath et al., in press), implying a nontrivial dust contribution to soil. Reheis and Kihl (1995) suggested that local deposition rates vary with fire activity and local soil disturbance in the region. If dust in the SGM is remobilized from soils locally, then it may not play a strong role in soil chemistry or weathering fluxes. However, dust sourced from the Mojave Desert to the North could have influenced soil elemental concentrations in high elevation or nearby soils. High elevation, eastern sites (E-U2, E-M3 and E-M4) display notably less negative tau K and tau Si values than low elevation hillslopes (Fig. 5), indicating less weathering losses and in some cases a net mass gain in these elements. Soils at Mount Williamson (E-M4) closest to the Mojave display positive tau K values suggesting a net mass gain in both crest and sideslope soils. The average composition fine grained Mojave dust (Reheis and Kihl, 1995; <50 μm; 74% SiO_2, 14% Al_2O_3, 2.2% Fe_2O_3, 1.0% CaO, 2.5% MgO, 3.1% Na, 2.2% K_2O) is distinct from bedrock chemistry at our sites, most notably for Mg and Fe, which are enriched in the highest elevation eastern soils but not in western soils (Table A4 of Supplementary material).

Our data suggest that dust likely does not play a strong role in overprinting soil chemistry and immobile enrichment at the low elevation western sites (Fig. 3A), where elemental concentrations likely reflect weathering processes. However, Ti and Zr concentrations in eastern soils (Fig. 3B) suggest that weathering alone cannot accurately reflect differences between soil and rock chemistry at three eastern sites. High variability in bedrock chemistry for both mobile and immobile elements for at least one of the eastern sites (E-M4; Table A1 of supplementary material) and the similar composition of E-U2 bedrock and dust measured by Reheis and Kihl (1995) also make it difficult to isolate the influence of dust, lithology, and weathering processes on soil geochemistry and to directly include dust deposition into the geochemical mass balance equations for weathering (Ferrier et al., in press).

4.3. Relationships between chemical weathering and erosion

For the calculation of weathering fluxes from measured elemental depletions in soils and saprolites, we focus on three western sites (W-U1, W-M1 and W-M2). Their close proximity, same bedrock lithology and similar climates and elevations minimize the variability in underlying chemical weathering controls mentioned in the previous section that may obscure the tectonic signature on weathering.

Saprolite weathering exceeds soil weathering rates in the SGM (Fig. 6; Table 2), similar to findings from other more slowly eroding landscapes (Anderson and Dietrich, 2001; Burke et al., 2007; Dixon et al., 2009a,b). Only at the three locations with highest physical erosion rates and thinnest soils, do soil production rates outpace saprolite production. This data suggests that at erosion rates less than ~300 t km^{-2} y^{-1} (~150 m Ma^{-1}), the downward propagation of the bedrock weathering front is able to keep pace with soil production and denudation. At higher erosion rates the saprolite mantle is lost, soils are formed directly from the mechanical disruption of fractured bedrock, and measurable weathering fluxes occur only within soils. This threshold for saprolite production may only apply for the narrow climate conditions of the SGM where mean annual precipitation is less than 120 cm y^{-1}, as wetter climates may be able to maintain deep weathering mantles at higher denudation rates.

Rates of weathering are highest at intermediate erosion rates (roughly ½ the maximum soil production rate, P_0; Figs. 6 and 7), in agreement with modeled fluxes predicted by the model of Ferrier and Kirchner (2008; Fig. 1A). Within this framework, weathering rates decrease with both decreasing and increasing rates of erosion from this maximum, due to the effects of lower mineral supply rates and shorter soil residence times respectively. Data from the SGM follow a similar pattern, with different slope morphologies describing separate portions of the rising and falling limbs of the model curves in Fig. 1. We find that marginal and upland hillslopes show two distinct relationships between erosion and weathering (Fig. 7A), and this difference is highlighted further if we categorize soils by slope gradient (Fig. 7C). Weathering rates on slopes <25° are positively correlated with erosion rates, while weathering rates on slopes >25° describe a negative relationship between erosion and weathering rates. Similarly, these morphologies exhibit distinct patterns between CDF and soil depth (Fig. 7B, D). Upland and low-gradient slopes show little predictable variation in CDFs with erosion rate, while marginal and high-gradient slopes show large variation in CDFs. As slope gradients approach a threshold between 20 and 30° on tectonically forced marginal hillslopes, a combination of thinner soils, faster erosion rates, and different erosion processes contribute to the distinct erosion–weathering relationships, and imply a clear signal of the hillslope weathering response to tectonics in the region.

Derived relationships between erosion, weathering and soil depth for distinct slope morphologies in the SGM are suggestive of the patterns derived from the mineral weathering model presented in Fig. 1. However, the data do not provide a strict validation for model predictions. Instead, we find the maximum weathering rates calculated in the SGM are lower than the model predicts, and there is notable variability in weathering rates along what would be the falling limb of the weathering–erosion curve. Furthermore, assumptions regarding parent material chemistry

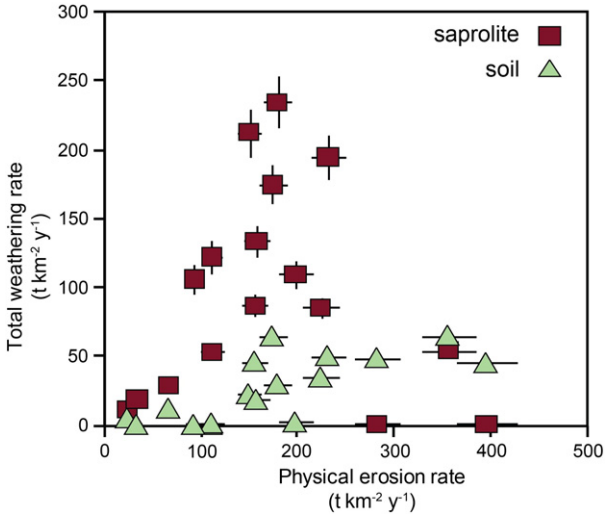

Fig. 6. Saprolite weathering (squares) composes the majority of weathering fluxes at western sites in the SGM, while soil weathering rates (triangles) play a minor role. At high erosion rates (>~250 t km^{-2} y^{-1}; ~100 m Ma^{-1}), soils directly overly bedrock, and saprolite weathering rates are therefore zero.

Table 2
Soil production, weathering and erosion rates.

Profile	CDF_{total}	CDF_{soil}	CDF_{sap}	D [a]	E [a]	W [a]	W_{soil} [a]	W_{sap} [a]
				($t\ km^{-2}\ y^{-1}$)	($t\ km^{-2}\ y^{-1}$)	($t\ km^{-2}\ y^{-1}$)	($t\ km^{-2}\ y^{-1}$)	($t\ km^{-2}\ y^{-1}$)
W-U1-1	0.40	0.18	0.27	38 ± 7	22 ± 4	16 ± 3	5 ± 1	11 ± 2
W-U1-2	0.30	0.01	0.30	164 ± 17	110 ± 12	54 ± 6	1 ± 0	53 ± 6
W-U1-3a	0.38	0.15	0.27	105 ± 13	63 ± 2	42 ± 1	11 ± 0	28 ± 1
W-U1-3b	0.34	0.00 (−0.03)	0.36 (0.38)[c]	50 ± 8	32 ± 5	18 ± 3	0 ± 0	18 ± 3
W-U1-4c	0.52	0.00 (−0.27)	0.52 (0.63)[c]	196 ± 19	91 ± 9	105 ± 11	0 ± 0	105 ± 11
W-M1-1	0.50	0.18	0.39	474 ± 22	231 ± 19	243 ± 20	49 ± 4	194 ± 16
W-M1-2	0.56	0.27	0.40	411 ± 23	173 ± 14	237 ± 19	64 ± 5	174 ± 14
W-M1-3	0.44	0.23	0.28	287 ± 21	155 ± 14	132 ± 12	45 ± 4	86 ± 8
W-M1-4	0.32	0.13	0.22	343 ± 22	224 ± 19	119 ± 10	34 ± 3	85 ± 7
W-M1-5	0.34	0.01	0.33	308 ± 22	197 ± 17	110 ± 10	2 ± 0	109 ± 9
W-M1-6	0.47	0.10	0.41	308 ± 22	157 ± 14	151 ± 13	18 ± 2	133 ± 12
W-M2-1[b]	0.51	–	–	231 ± 20	109 ± 10	121 ± 12	–	–
W-M2-2	0.58	0.14	0.51	441 ± 23	179 ± 14	263 ± 21	29 ± 2	233 ± 19
W-M2-3	0.60	0.13	0.54	382 ± 22	149 ± 12	233 ± 19	22 ± 2	211 ± 18
W-M2-4	0.12	0.17	0.00	331 ± 22	283 ± 24	48 ± 4	48 ± 4	0 ± 0
W-M2-5	0.22	0.15	0.08	474 ± 22	357 ± 29	117 ± 9	64 ± 5	53 ± 4
W-M2-6	0.07	0.16	0.00	441 ± 23	397 ± 32	44 ± 4	44 ± 4	0 ± 0

[a] Errors on denudation rates reflect uncertainty on the reported soil production function (Eq. (7)). All other errors are propagated from analytical uncertainty on [Zr] (~5% relative error) and on denudation rates.
[b] Saprolite sample missing; no corresponding chemistry data.
[c] Saprolite [Zr] at these sites are higher than overlying soil concentrations. Here, we have calculated rates assuming the CDF_{total} is representative of total weathering. Data in parentheses reflect CDFs if saprolite [Zr] is representative. If measured CDF_{sap} instead represents the correct total weathering extent, then W and E would be 120 and 69 $t\ km^{-2}\ y^{-1}$ respectively at W-U1-4. Calculated rates at W-U1-3b are unaffected. All elemental concentrations provided in Tables A1–A3 of the Supplementary material.

are nontrivial for derived rates and extents of weathering at western sites in the SGM and require some caution. Ti–Zr ratios and concentrations suggest bedrock sampled at W-M2 is representative of unweathered parent material at two nearby sites; however, it is possible that bedrock within the same granitic pluton is widely variable geochemically. The derivation of a humped relationship between weathering and erosion rates (Fig. 7A) is dependent on our accurate characterization of weathering rates at the upland site W-U1, which are the lowest in the region. The most novel result from our study, the observation of decreasing chemical weathering extents and rates shown in Fig. 8A and 8C, is not dependent on these assumptions however, since this decrease is observed at site W-M2, where parent material is well constrained.

4.4. Kinetic limitation and the weathering response to uplift

A number of independent observations suggest that weathering at sites in the SGM is kinetically limited: 1) CDF and tau values change downslope, even on low-gradient portions of the landscape, potentially associated with differences in soil residence times and the availability of water; 2) chemical weathering intensities decrease across 25° slopes with a number of associated changes in both hillslope morphology and transport processes; 3) elevational differences suggest weathering is sensitive to climate or dust deposition. Chemical weathering extents measured from weathered residuum (for example, using the CDF or tau values) would be insensitive to climate, dust deposition, residence time and erosion rates only if the weathering regime is supply limited, such that minerals have time to fully weather despite the addition of fresh minerals or differences in kinetic constraints. Therefore, the direct imprint of climate, dust deposition, or soil residence times on chemical depletions would only be discernable in a kinetically limited system. Furthermore, the presence of abundant plagioclase feldspars in first order basins in the western SGM (modal average 51%; Critelli et al., 1997) indicates that mineral weathering remains kinetically limited through the transport pathway of the mineral from bedrock, to soils, to the river basin. That mineral weathering is likely kinetically limited in the SGM poses both a help and hindrance when one wants to determine the primary controls on mineral weathering, since if weathering is kinetically limited it has a greater likelihood of being sensitive to multiple controls (hydrology, temperature, acidity, transport time, etc.). Therefore, it may not be surprising that our data are only suggestive of – and do not strictly validate – the model in Fig. 1, which predicts weathering only under changing erosion rates. A single set of input parameters

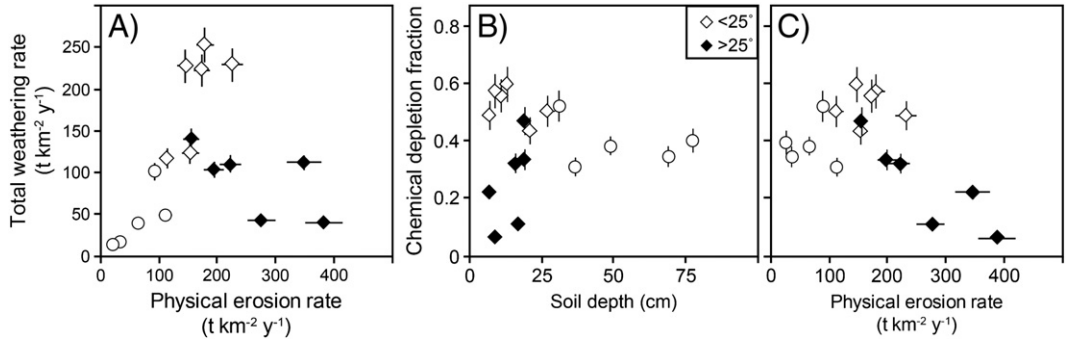

Fig. 7. Chemical weathering rates at three sites in the Western SGM increase and then decrease with increasing erosion rates (A,), and weathering depletions decrease as soils thin (B) and erosion rates increase (C). Chemical weathering rates for upland (circles) hillslopes increase with erosion rate while chemical depletions are relatively invariant (B, C). Marginal hillslopes (diamonds) describe different relationships in these plots, suggesting that both chemical weathering rates and extents decrease with increasing erosion rates. These differences are further highlighted when one compares low-gradient (<25°; white) and high-gradient (>25°; black) portions of the hillslopes. These data follow similar trends to those predicted by the model of Ferrier and Kirchner (2008) in Fig. 1.

(Eqs. (9)–(10), Table A5 of supplementary material) derive a single set of curves (Fig. 1) that are unable to account for local-hillslope or across-landscape variability in biologic, hydrologic or climatic conditions that could influence mineral dissolution kinetics.

We identify two important transitions in the relationship between erosion rates and weathering rates from both the model and our data. The first transition is from supply limited weathering to kinetically limited weathering. The modeled curves suggest that this transition in the SGM occurs at very low erosion rates ~10 $t\,km^{-2}\,y^{-1}$, as the relationship between erosion and weathering rates becomes non-linear and CDFs begin to decrease (Fig. 1A). Across this threshold, weathering rates continue to increase because the benefits of increasing mineral supply rates offset the negative effects of decreasing soil residence times. The second important transition reflects a threshold within kinetic limitation as the benefits from mineral supply are exceeded by the effects of decreasing soil residence time. As weathering rates reach their zenith and erosion rates continue to increase, weathering rates decline as the effect of shortening residence times outweigh the effect of increasing mineral supply rates (Figs. 1 and 7). The transition from kinetic limitation to kinetic control has not been previously identified with field data. Our results suggest that in the SGM, this transition occurs with tectonic forcing as upland hillslopes alter their morphology and hillslope gradients approach threshold slopes. These chemical patterns across the landscape complement previously recognized physical patterns that occur as slope gradients approach 30° and erosion processes transition from creep to landslide dominated erosion (DiBiase et al., 2009).

5. Conclusions

In this paper we quantify chemical weathering across hillslopes in the San Gabriel Mountains (SGM) of California. These hillslopes experience a range of morphologies likely associated with the response to a propagating wave of incision across the SGM. Data from both upland hillslopes above river knickpoints and hillslopes at the margin of the incising terrain suggest that chemical weathering across the SGM is kinetically limited and controlled by the combination of soil residence times, water availability and dust deposition. Soil weathering extents are widely variable at both a hillslope scale and at a landscape scale, inconsistent with the prediction that supply-limited hillslopes will display relatively uniform weathering extents across their soils (Fig. 1B). Upland, low-relief hillslopes have slopes <20° and generally show increasing soil weathering extents downslope. We infer that the accumulation of moisture coupled with weathering during downslope soil transport results in increased chemical weathering downslope on low-gradient slopes. Soil weathering decreases midslope on marginal hillslopes, coincident with a downslope morphologic and process transition as gradients exceed 25°. We attribute the decrease in weathering extents (as shown by CDFs and tau values) across these slope transitions to a number of coincident changes in hillslope morphology and erosion: a shift to faster erosion rates, thinner soils and a change in transport processes as soils become rockier. These results are consistent with a kinetic limitation on soil weathering, and together suggest that there is a strong tectonic control on chemical weathering rates on soil-mantled hillslopes across the SGM. Lastly, our results corroborate the model by Ferrier and Kirchner (2008) and suggest that weathering fluxes in tectonically active landscapes may be low due to short soil residence times, shallow soil depths and high erosion rates. This data identifies a kinetic control regime (Fig. 1) that has not been previously validated with field data. An important implication of this regime is that tectonic uplift may in fact retard chemical weathering rates by increasing erosion rates beyond some threshold, and therefore may not stimulate increased CO_2 drawdown by silicate weathering. Whether this regime can be identified in other landscapes, including those in wetter climates, will test whether this implication is relevant at a global scale. Therefore, this work highlights the pressing need for more field-based studies that quantify soil weathering in rapidly eroding landscapes.

Acknowledgments

We are grateful to G. Hilley, one anonymous reviewer and editor R. Carlson for their constructive and thoughtful reviews. M. Jungers, M. Rossi and J. Walsh assisted in the field. Many thanks to K. Norton, H. Wittmann, T. Schildgen and others for insight and input that helped to improve our manuscript and thinking. This work was supported with funding from NSF-Geomorphology and Landuse Dynamics (AMH and KXW).

Appendix A. Supplementary data

Supplementary data to this article can be found online at doi:10.1016/j.epsl.2012.01.010.

References

Alf, R.M., 1948. A mylonite belt in the southeastern San Gabriel Mountains, California. Geol. Soc. Am. Bull. 59, 1101–1120.
Anderson, S.P., Dietrich, W.E., 2001. Chemical weathering and runoff chemistry in a steep headwater catchment. Hydrol. Processes 15, 1791–1815.
Barth, A.P., 1990. Mid-crustal emplacement of Mesozoic plutons, San Gabriel Mountains, California, and implications for the geologic history of the San Gabriel terrace. In: Anderson, J.L. (Ed.), Geological Society of America, Memoir, pp. 33–45.
Berner, R.A., Lasaga, A.C., Garrels, R.M., 1983. The carbonate–silicate geochemical cycle and its effect on atmospheric carbon dioxide over the past 100 million years. Am. J. Sci. 283, 641–683.
Blythe, A.E., Burbank, D.W., Farley, K., Fielding, E., 2000. Structural and topographic evolution of the central Transverse Ranges, California, from apatite fission-track, (U–Th)/He and digital elevation model analyses. Basin Res. 12, 97–114.
Blythe, A.E., House, M.A., Spotila, J.A., 2002. Low-temperature thermochronology of the San Gabriel and San Bernardino Mountains, southern California: constraining structural evolution. Geol. Soc. Am. Spec. Pap. 365, 231–250.
Brimhall, G.H., Chadwick, O.A., Lewis, C.J., Compston, W., Williams, I.S., Danti, K.J., Dietrich, W.E., Power, M.E., Hendricks, D., Bratt, J., 1992. Deformational mass transport and invasive processes in soil evolution. Science 255, 695–702.
Burke, B.C., Heimsath, A.M., White, A.F., 2007. Coupling chemical weathering with soil production across soil-mantled landscapes. Earth Surf. Processes Landforms 32, 853–873.
Chadwick, O.A., Brimhall, G.H., Hendricks, D.M., 1990. From a black to a gray box — a mass balance interpretation of pedogenesis. Geomorphology 3, 369–390.
Chamberlain, C.P., Waldbauer, J.R., Jacobson, A.D., 2005. Strontium, hydrothermal systems and steady-state chemical weathering in active mountain belts. Earth Planet. Sci. Lett. 238, 351–366.
Critelli, S., Le Pera, E., Ingersoll, R.V., 1997. The effects of source lithology, transport, deposition and sampling scale on the composition of southern California sand. Sedimentology 44, 653–671.
DiBiase, R.A., Whipple, K.X., Heimsath, A.M., Ouimet, W.B., 2009. Landscape form and millennial erosion rates in the San Gabriel Mountains, CA. Earth Planet. Sci. Lett. 289, 134–144.
Dixon, J.L., Heimsath, A.M., Kaste, J., Amundson, R., 2009a. Climate-driven processes of hillslope weathering. Geology 37, 975–978.
Dixon, J.L., Heimsath, A.M., Amundson, R., 2009b. The critical role of climate and saprolite weathering in landscape evolution. Earth Surf. Processes Landforms 34, 1507–1521.
Fernandes, N.F., Dietrich, W.E., 1997. Hillslope evolution by diffusive processes: the timescale for equilibrium adjustments. Water Resour. Res. 33, 1307–1318.
Ferrier, K.L., Kirchner, J.W., 2008. Effects of physical erosion on chemical denudation rates: a numerical modeling study of soil-mantled hillslopes. Earth Planet. Sci. Lett. 272, 591–599.
Ferrier, K.L., Kirchner, J.K., Finkel, R.C., 2011. Estimating millennial-scale rates of dust incorporation into eroding hillslope regolith using cosmogenic nuclides and immobile weathering tracers. J. Geophys. Res. Earth Surf. 116, F03022.
Gabet, E.J., 2007. A theoretical model coupling chemical weathering and physical erosion in landslide-dominated landscapes. Earth Planet. Sci. Lett. 264, 259–265.
Gabet, E.J., Mudd, S.M., 2009. A theoretical model coupling chemical weathering rates with denudation rates. Geology 37, 151–154.
Gaillardet, J., Dupre, B., Louvat, P., Allegre, C.J., 1999. Global silicate weathering and CO_2 consumption rates deduced from the chemistry of large rivers. Chem. Geol. 159, 3–30.
Green, E.G., Dietrich, W.E., Banfield, J.F., 2006. Quantification of chemical weathering rates across an actively eroding hillslope. Earth Planet. Sci. Lett. 242, 155–169.
Heimsath, A.M., Dietrich, W.E., Nishiizumi, K., Finkel, R.C., 1997. The soil production function and landscape equilibrium. Nature 388, 358–361.
Heimsath, A.M., Dietrich, W.E., Nishiizumi, K., Finkel, R.C., 1999. Cosmogenic nuclides, topography, and the spatial variation of soil depth. Geomorphology 27, 151–172.

Heimsath, A.M., DiBiase, R.A., Whipple, K.X., 2012. Soil production limits and the transition to bedrock dominated landscapes. Nat. Geosci. advance online publication (DOI:10.1038/NGEO1380).
Hilley, G.E., Porder, S., 2008. A framework for predicting global silicate weathering and CO_2 drawdown rates over geologic time-scales. Proc. Natl. Acad. Sci. U. S. A. 105, 16855–16859.
Hilley, G.E., Chamberlain, C.P., Moon, S., Porder, S., Willett, S.D., 2010. Competition between erosion and reaction kinetics in controlling silicate-weathering rates. Earth Planet. Sci. Lett. 293, 191–199.
Howard, A.D., Dietrich, W.E., Seidl, M.A., 1994. Modeling fluvial erosion on region to continental scales. J. Geophys. Res. Solid Earth 99, 13971–13986.
Hren, M.T., Hilley, G.E., Chamberlain, C.P., 2007. The relationship between tectonic uplift and chemical weathering rates in the Washington Cascades: field measurements and model predictions. Am. J. Sci. 307, 1041–1063.
Jacobson, A.D., Blum, J.D., Chamberlain, C.P., Craw, D., Koons, P.O., 2003. Climatic and tectonic controls on chemical weathering in the New Zealand Southern Alps. Geochim. Cosmochim. Acta 67, 29–46.
Kiefer, J.W., Fenn, M.E., 1997. Using vector analysis to assess nitrogen status of ponderosa and Jeffrey pine along deposition gradients in forests of southern California. For. Ecol. Manage. 94, 47–59.
Kurtz, A.C., Derry, L.A., Chadwick, O.A., 2001. Accretion of Asian dust to Hawaiian soils: isotopic, elemental, and mineral mass balances. Geochim. Cosmochim. Acta 65, 1971–1983.
Lavé, J., Burbank, D., 2004. Denudation processes and rates in the Transverse Ranges, southern California: erosional response of a transitional landscape to external and anthropogenic forcing. J. Geophys. Res. 109 F01006.
Millot, R., Gaillardet, J., Dupré, B., Allègre, C.J., 2002. The global control of silicate weathering rates and the coupling with physical erosion: new insights from rivers of the Canadian Shield. Earth Planet. Sci. Lett. 196, 83–98.
Molnar, P., Anderson, R.S., Anderson, S.P., 2007. Tectonics, fracturing of rock, and erosion. J. Geophys. Res. Earth Surf. 112, F03014.
Morton, D.M., Miller, F.K., 2006. Geologic map of the San Bernardino and Santa Ana $30' \times 60'$ quadrangles, California. U.S. Geological Survey Open-File Report.
Mudd, S.M., Furbish, D.J., 2007. Responses of soil-mantled hillslopes to transient channel incision rates. J. Geophys. Res. Earth Surf. 112, F03S18.
Muir, J.W., Logan, J., 1982. Eluvial/illuvial coefficients of major elements and the corresponding losses and gains in three soil profiles. Journal of Soil Science 33, 295–308.
Norton, K.P., von Blanckenburg, F., 2010. Silicate weathering of soil-mantled slopes in an active Alpine landscape. Geochim. Cosmochim. Acta 74, 5243–5258.
Ouimet, W.B., Whipple, K.X., Granger, D.E., 2009. Beyond threshold hillslopes: channel adjustment to base-level fall in tectonically active mountain ranges. Geology 37, 579–582.
Padgett, P.E., Bytnerowicz, A., 2001. Deposition and adsorption of the air pollutant HNO_3 vapor to soil surfaces. Atmos. Environ. 35, 2405–2415.
Porder, S., Hilley, G.E., Chadwick, O.A., 2007. Chemical weathering, mass loss, and dust inputs across a climate by time matrix in the Hawaiian Islands. Earth Planet. Sci. Lett. 258, 414–427.
Reheis, M.C., Kihl, R., 1995. Dust deposition in southern Nevada and California, 1984–1989: relations to climate, source area, and source lithology. J. Geophys. Res. 100, 8893–8918.
Reinhardt, L.J., Bishop, P., Hoey, T.B., Dempster, T.J., Sanderson, D.C.W., 2007. Quantification of the transient response to base-level fall in a small mountain catchment: Sierra Nevada, southern Spain. J. Geophys. Res. 112, F03S05.
Riebe, C.S., Kirchner, J.W., Granger, D.E., Finkel, R.C., 2001. Strong tectonic and weak climatic control of long-term chemical weathering rates. Geology 29, 511–514.
Riebe, C.S., Kirchner, J.W., Finkel, R.C., 2004. Erosional and climatic effects on long-term chemical weathering rates in granitic landscapes spanning diverse climate regimes. Earth Planet. Sci. Lett. 224, 547–562.
Riggan, P.J., Lockwood, R.N., Lopez, E.N., 1985. Deposition and processing of airborne nitrogen pollutants in Mediterranean-type ecosystems of Southern-California. Environ. Sci. Technol., 19, pp. 781–789.
Ruddiman, W.F., Raymo, M.E., Prell, W.L., Kutzbach, J.E., 1997. The uplift–climate connection: a synthesis. In: Ruddiman, W.F. (Ed.), Tectonic Uplift and Climate Change. Plenum Press, New York, pp. 471–515.
Spotila, J.A., House, M.A., Blythe, A.E., Niemi, N.A., Bank, G.C., 2002. Controls on the erosion and geomorphic evolution of the San Bernardino and San Gabriel Mountains, southern California. Geol. Soc. Am. Spec. Pap. 365, 205–230.
Stallard, R.F., Edmond, J.M., 1983. Geochemistry of the Amazon: II. The influence of the geology and weathering environment in the dissolved load. J. Geophys. Res. 88, 9671–9688.
Tonnesen, G., Wang, Z., Omary, M., Chien, C.J., 2007. Assessment of nitrogen deposition: modeling and habitat assessment. California Energy Commission, PIER Energy-Related Environmental Research. CEC-500-2006-032.
Waldbauer, J.R., Chamberlain, C.P., 2005. Influence of uplift, weathering and base cation supply on past and future CO_2 levels. In: Ehleringer, J.R., Cerling, T.E., Dearing, M.D. (Eds.), History of Atmospheric CO_2 and Its Effects on Plants, Animals and Ecosystems. Springer Verlag, Berlin, pp. 166–184.
West, A.J., Galy, A., Bickle, M., 2005. Tectonic and climatic controls on silicate weathering. Earth Planet. Sci. Lett. 235, 211–228.
Whipple, K.X., Tucker, G.E., 1999. Dynamics of the stream-power river incision model: implications for height limits of mountain ranges, landscape response timescales, and research needs. J. Geophys. Res. 104, 17661–17674.
White, A.F., Blum, A.E., 1995. Effects of climate on chemical weathering in watersheds. Geochim. Cosmochim. Acta 59, 1729–1747.
Yerkes, R.F., Campbell, R.H., 2005. Preliminary Geologic Map of the Los Angeles $30' \times 60'$ Quadrangle, Southern California. U.S. Geological Survey Open-File Report.
Yoo, K., Amundson, R., Heimsath, A.M., Dietrich, W.E., Brimhall, G.H., 2007. Integration of geochemical mass balance with sediment transport to calculate rates of soil chemical weathering and transport on hillslopes. J. Geophys. Res. 112, F02013.